frontiers | Frontiers in Earth Science

TYPE Original Research
PUBLISHED 30 July 2024
DOI 10.3389/feart.2024.1347243

OPEN ACCESS

EDITED BY
Ryan Mathur,
Juniata College, United States

REVIEWED BY
Liang Qiu,
China University of Geosciences, China
Hua-Wen Cao,
Chengdu University of Technology, China

*CORRESPONDENCE
Runsheng Han,
554670042@qq.com

RECEIVED 30 November 2023
ACCEPTED 24 June 2024
PUBLISHED 30 July 2024

CITATION
Wu J, Han R, Zhang Y, Wu P, Gong H, Wang L, Cheng G, Li X, Yang Y and Mi Y (2024), Porosity–permeability characteristics and mineralization–alteration zones of the Maoping germanium-rich lead–zinc deposit in SW China.
Front. Earth Sci. 12:1347243.
doi: 10.3389/feart.2024.1347243

Porosity–permeability characteristics and mineralization–alteration zones of the Maoping germanium-rich lead–zinc deposit in SW China

Jianbiao Wu, Runsheng Han*, Yan Zhang, Peng Wu, Hongsheng Gong, Lei Wang, Gong Cheng, Xiaodong Li, Yixuan Yang and Yaya Mi

Kunming University of Science and Technology, Geological Survey Center for Nonferrous Metals Resources, Southwest Institute of Geological Survey, Kunming, China

The Maoping superlarge germanium-rich lead–zinc deposit is a typical nonmagmatic hydrothermal deposit that is structurally controlled in the Sichuan–Yunnan–Guizhou lead–zinc polymetallic metallogenic area. The orebodies are distributed in several formations. This paper is based on large-scale alteration mapping combined with porosity and permeability measurements. We delineated the mineralization–alteration zones of different ore-bearing formations, explored the geological significance of porosity and permeability, and proposed prospecting directions. The research results indicate that during the mineralization period, the ore-forming metal fluids migrated from the deep part of the SSW region to the shallow part of the NNE region along the ore-guiding structure (Maoping Fault). Through the ore distribution structure, depressurization boiling occurred in the open space of the NE-trending interlayered sinistral compressive–torsional faults in several ore-bearing formations, resulting in fluid precipitation and the formation of different brecciated hot-melt dolomite lead–zinc mineralization zones. From the orebody to the wallrock, the C_2w Formation and D_3zg Formation are divided into four different mineralization–alteration zones. Tectonic activity affects the properties, migration, and precipitation of fluids, thereby controlling the alteration characteristics generated during fluid migration and thus changing the porosity and permeability. The porosity and permeability of strata on the NW flank of the anticline are greater than those of strata on the SE flank. On the NW flank, the greater the degree of mineralization–alteration is, the greater the porosity and permeability are, and the porosity of the orebody is lower than that during dolomitization. Finally, we believe that the NW flank of the anticline is an important area for prospecting. The pyrite + striped altered dolomite zone (Zones II–III) in the C_2w limestone and the pyrite + strong dolomite zone (Zones II–III) in the D_3zg dolomite are important prospecting indicators.

KEYWORDS

porosity and permeability, mineralization-alteration zones, metallogenic patterns, prospecting directions, Maoping superlarge germanium-rich lead-zinc deposit, Sichuan-Yunnan-Guizhou lead-zinc polymetallic metallogenic area

1 Introduction

In the next 2 decades, human consumption of base metals, such as lead, zinc and copper, will exceed the total production of these metals in human history (Ali et al., 2017; Hoggard et al., 2020). To date, nearly 300 germanium-rich lead–zinc (silver) deposits (occurrences) have been discovered in the Sichuan–Yunnan–Guizhou lead–zinc polymetallic metallogenic area in China. These lead–zinc deposits have produced more than 20 million tons of lead and zinc, and the deposits are exceptionally high grade and rich in associated germanium and silver (Han et al., 2022; 2023). This area is the largest lead–zinc industrial base and the world's primary germanium production base (Han et al., 2022). With the long-term depletion of shallow mineral resources, there is a need for better targeted exploration to help improve research on deeply buried deposits and find deep mineral resources to maintain the supply of base metals for humankind.

Previous studies on mineralization–alteration zones have provided an important basis for the discovery of several deposits and orebodies in the Sichuan–Yunnan–Guizhou lead–zinc polymetallic metallogenic area (Wen et al., 2014; Chen et al., 2016; Zhao et al., 2016). The Maoping superlarge germanium-rich lead–zinc deposit is a typical deposit in the Sichuan–Yunnan–Guizhou lead–zinc polymetallic metallogenic area and is controlled by structure and favorable lithological associations (Han et al., 2019; Han et al., 2022; Wu et al., 2023), and orebodies occur in several ore-bearing formations (Han et al., 2022). Moreover, the mineralization–alteration characteristics and zoning patterns vary among different ore-bearing formations. This seriously restricts the prediction and positioning of deep hidden orebodies in different ore-bearing formations of this deposit and even this type of deposit.

In this study, a large-scale alteration mapping method is used to conduct detailed mapping and sampling on four ore blocks, nine planes, and several profiles of the Maoping lead–zinc deposit. The mineralization–alteration type, strength, mineral combination, structure, and other characteristics are analyzed, and the mineralization–alteration zones are identified. The porosity and permeability characteristics of 106 rocks (minerals) in different mineralization–alteration zones on the two flanks of the Maomaoshan anticline are analyzed. The geological significance of the porosity and permeability and proposed prospecting directions are explored. This study provides a theoretical basis for the deep exploration of other similar hydrothermal deposits.

2 Geological setting

The Maoping superlarge germanium-rich lead–zinc deposit is a typical superlarge CNHT lead–zinc deposit in the

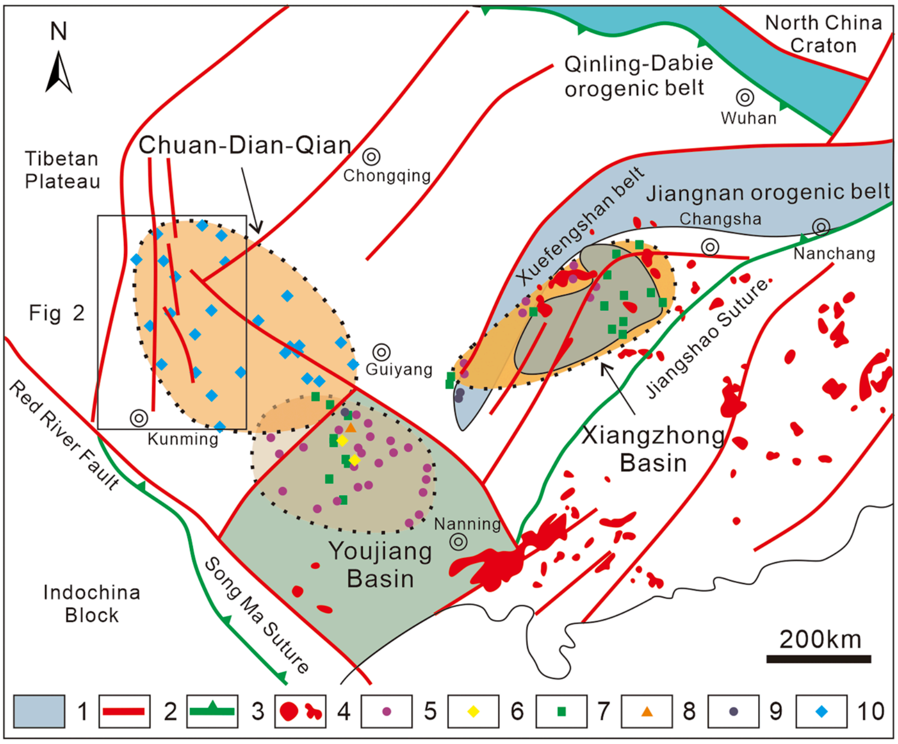

FIGURE 1
A simplified geological map of the South China Block and adjacent regions showing the structural framework and the distribution of ore deposits in the Yangtze Block (modified from Yan et al., 2003; Qiu et al., 2016; Hu et al., 2017; Wu et al., 2020). 1—Proterozoic basement; 2—Fault/Main boundary fault; 3—Suture zone; 4—Triassic granitoids; 5—Gold deposit; 6—Realgar deposit; 7—Stibnite deposit; 8—Tin deposit; 9—Mercury deposit; 10—Lead–zinc deposit.

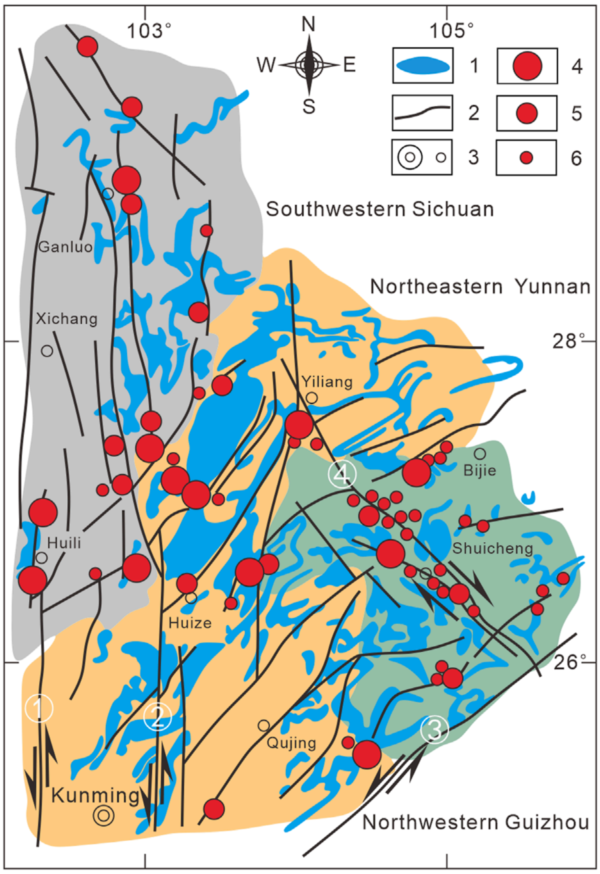

FIGURE 2
Distribution of the main thrust–fold belts and deposits in the Sichuan–Yunnan–Guizhou zinc–lead poly–metallic mineralization domain (SYGD) (Wang et al. 2004; Han et al. 2019). 1—The upper permian basalt Formation; 2—Main fault; 3—Provincial boundaries; 4—Provincial capital and city/county; 5—Large and medium–sized deposits; 6—Small deposits; ①–Lvzhijiang fault, ②–Xiaojiang fault, ③–Weining–Shuicheng fault, ④–Ziyun–Yadu fault.

Sichuan–Yunnan–Guizhou lead–zinc polymetallic metallogenic area on the southwestern margin of the Yangtze block (Figure 1) (Yan et al., 2003; Qiu et al., 2016; Hu et al., 2017; Wu et al., 2020). The deposit is located at the intersection of the NE-trending Huize–Niujie oblique thrust–strike-slip fault–fold belt, the SN-trending Qujing–Zhaotong concealed fault zone, and the NW-trending Ziyun–Yadu deep fault zone (Figure 2) (Wang et al., 2004; Han et al., 2019). The deposit is mainly controlled by the NE-trending Maoping compressive–torsional fault (the names of these sequential transformation structural planes indicate that their mechanical properties are mainly composed of compressional structures and, secondarily, torsional structures) and the Maomaoshan anticline in its hanging wall (Figure 3). The main structures in the deposit area are NE-trending, NW-trending and N–S-trending structures, with the NE-trending interlayered sinistral compressive–torsional fault dominating (Figure 3). The deposit area is mainly composed of Devonian, Carboniferous, and Permian carbonate–clastic rock series, which are mostly in parallel unconformable or conformable contact. The orebodies mainly occur in the grayish-white–dark gray fine–medium crystalline dolomite of the upper Devonian Zaige Formation (D_3zg), the light flesh-red or grayish-white massive fine crystalline dolomitic limestone of the lower Carboniferous Baizuo Formation (C_1b), and the light gray–dark gray medium-to thick-layered dolomitic limestone of the upper Carboniferous Weining Formation (C_2w) (Figures 3, 4). The magmatic rocks are mainly in the upper Permian Basalt Formation. The deposit is composed of the No. I, II, III and VI orebodies in the ore block to the east of the Luoze River and the Shuilu, Qiancengdong and Hongjianshan ore blocks to the west of the Luoze River (Figure 3). The orebodies are mainly lenticular, vein-like and stratiform-like. The main ore minerals are galena, sphalerite and pyrite, etc., and the gangue minerals are dolomite, calcite, minor quartz and barite, etc. The ore structures are compact, massive, disseminated, vein-like, veinlet-like, massive and stellate, and the ore textures are mainly granular and metasomatic. The main types of wallrock alteration include pyritization, ferritization, dolomitization, calcification and silicification.

3 Materials and methods

In this study, a large-scale alteration mapping method was used to conduct detailed mapping and systematically determine the mineralization–alteration zoning characteristics within different ore-bearing strata of the deposit. On the basis of the systematic study of mineralization–alteration characteristics (Table 1), the porosity and permeability of representative rocks were analyzed. The rock samples for the porosity and permeability study were collected from the NW and SE flanks of the Maomaoshan anticline, and they were collected from the surface of the mining area and the mining tunnels to obtain a total of 106 pieces. Among them, 58 fresh samples were collected from different lithological formations on the surface. A total of 48 samples from the tunnel were collected from the 32–33+first line of 670 m of the H8 orebody in the Hexi Hongjianshan ore block, the 34+first line of 610 m of the H8 orebody in the Hexi Hongjianshan ore block, the 18th line of the 755 m of the Q1 orebody in the Hexi Qiancengdong ore block, the second line of the 670 m of the S1 orebody in the Hexi Shuilu ore block, the 116th line of the 760 m of the I-7 orebody in the Hedong ore block, the 98+first line of the 683 m of the I-6 orebody in the Hedong ore block, the 92nd line of the 670 m in the Hedong ore block, the 96–112nd line of the 610 m of the I-6 orebody in the Hedong ore block, the stope of the 490 m of the I-8 orebody in the Hedong ore block, the stope of the 430 m of the I-8 orebody in the Hedong ore block, the 90–96th lines of the 370 m of the I-8 orebody in the Hedong ore block, and the 98–104th lines of the 310 m of the I-8 orebody in the Hedong ore block. The samples were tested for porosity and permeability by using a QKY-2 gas porosity tester and a STY-2 gas permeability tester at the China University of Petroleum (Beijing). The former had a measurement accuracy of 0.5%, while the latter had a relative error of less than 5%. Nitrogen was used as the working medium in the experiment, and the test was repeated five times. The average value was taken as the result for porosity or permeability (Table 2).

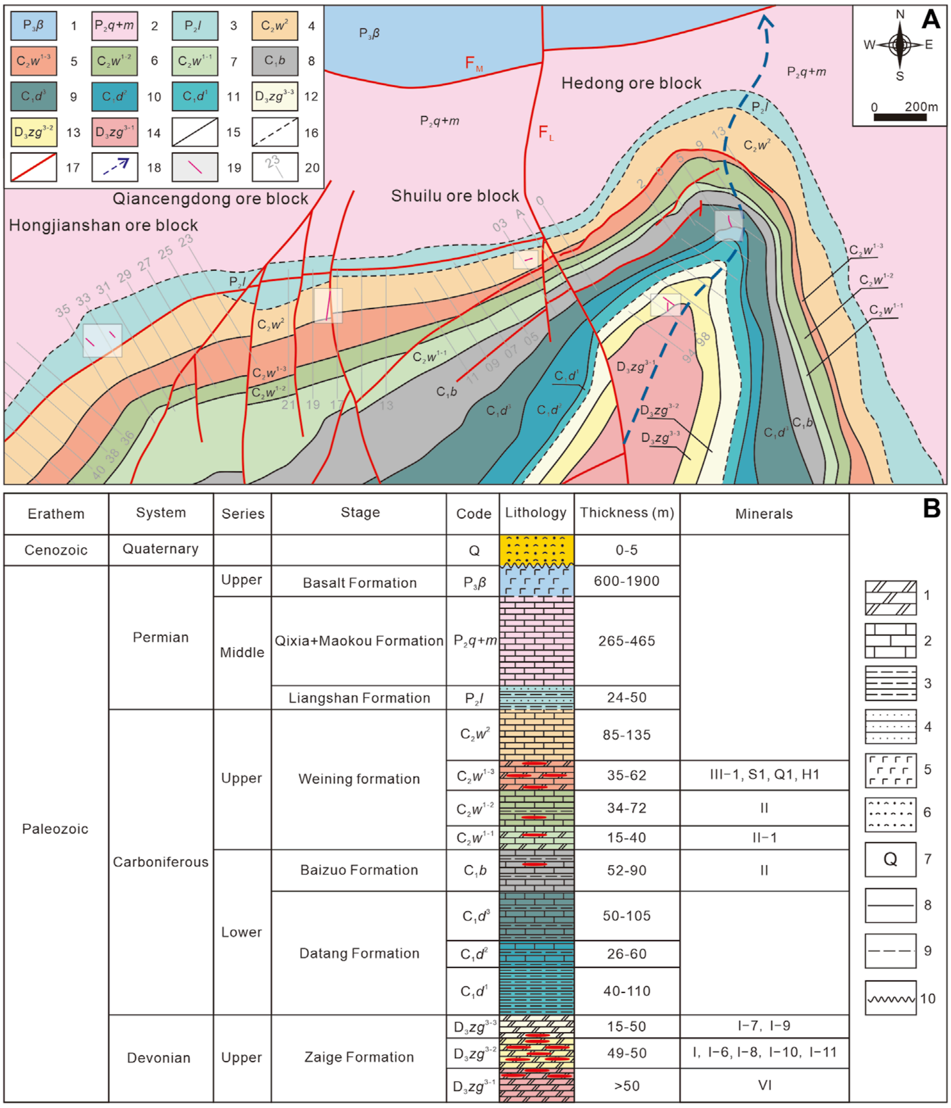

FIGURE 3
Geological map, actual material plane projection map **(A)** and Stratigraphic histogram of the Maoping lead-zinc deposit **(B)** (Wu et al. 2024). Figure 3A: 1—Upper Permian Basalt Formation; 2—Middle Permian Qixia+Maokou Formation; 3—Middle Permian Liangshan Formation; 4—Upper Carboniferous Weining Formation; 5—The third section of the first layer of the Weining Formation in the Upper Carboniferous; 6—The second section of the first layer of the Weining Formation in the Middle Carboniferous; 7—The first section of the first layer of the Weining Formation in the Upper Carboniferous; 8—Lower Carboniferous Baizuo Formation; 9—The third layer of the Lower Carboniferous Datang Formation; 10—The second layer of the Lower Carboniferous Datang Formation; 11—The first layer of the Lower Carboniferous Datang Formation; 12—The third layer of the third member of the Upper Devonian Zaige Formation; 13—The second layer of the third section of the Upper Devonian Zaige Formation; 14—The first layer of the third section of the Upper Devonian Zaige Formation; 15—Integrated contact; 16—Parallel unconformity contact; 17—Fault; 18—Anticline axis; 19—The location of the cross sections; 20—Exploration lines and numbering. Figure 3B: 1—Dolomite; 2—Limestone; 3—Mudstone; 5—Sandstone; 5—Basalt; 6—Residual matter; 7—Stratum code; 8—Integrated contact; 9—False integration contact; 10—Angular unconformity contact.

4 Results

4.1 Characteristics and zones of mineralization–alteration

The mineralization of the Maoping lead–zinc deposit is mainly that of galena and sphalerite. The wallrock alteration type is relatively simple, and the intensity changes and zoning are obvious. These mainly include pyritization, (iron) dolomitization and calcification. The main alteration characteristics are as follows (Figures 5–7).

Pyritization: Pyritization is mainly distributed in the dolomite, calcite, joints and faults near the ore in massive structures, disseminated structures, masses, veins, and veinlets, and pyrite is also common in the orebodies. The intensity of pyritization is related to its distance from the orebody. The pyritization near the orebodies is strong, and the pyritization far from the orebodies gradually weakens. In addition, the pyritization is also related to

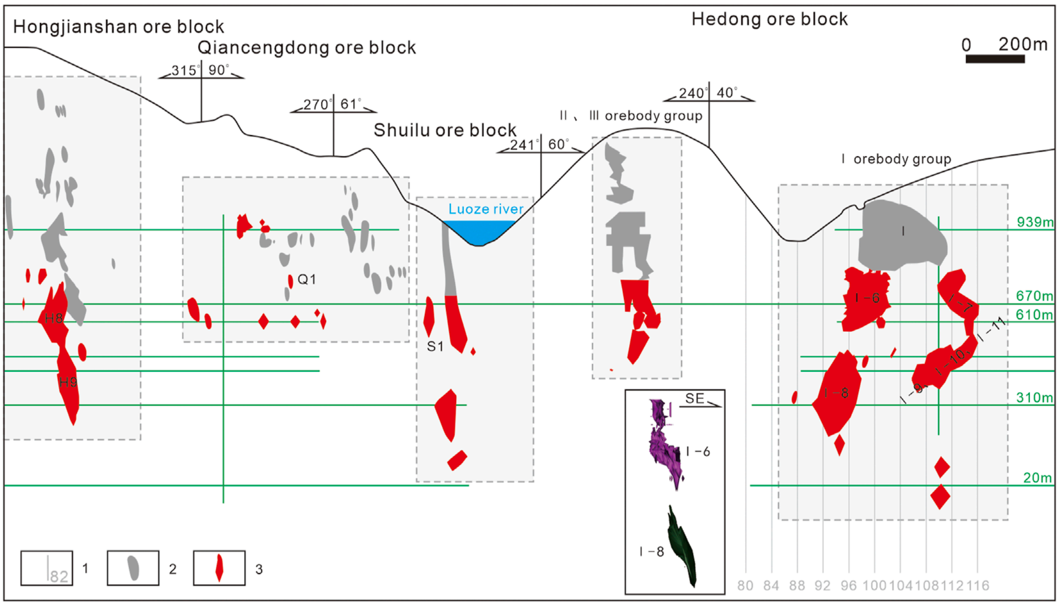

FIGURE 4
Orebody longitudinal projection map of Maoping lead–zinc deposit. 1—Exploration line and number; 2—Mined out orebodies; 3—Known orebodies.

elevation, and deep pyritization is obviously stronger than shallow pyritization.

Dolomitization: Due to the influence of hydrothermal activity, the original dolomite limestone or dolomite is recrystallized, resulting in a significant increase in porosity, which is beneficial for hydrothermal activity and mineralization, thus leading to the formation of altered dolomite. Dolomite is mainly found in striped structures, veins, masses, veinlets, and irregular structures; is mainly distributed on the sides of orebodies and the sides of interlayer faults; and has a semi-idiomorphic granular framework. The particle sizes are 0.2–1 mm, and the color is diverse—mainly white, gray–white, beige, and flesh red; in addition, corrosion holes and crystal cavities have developed. Dolomitization is more evident in the C_2w dolomitic limestone, where it appears as a stripe; the D_3zg dolomite mainly appears in a rice-grain-type form, with the presence of long-axis parallel interlayer faults.

Calcification: Calcification is present mainly in the forms of stockwork, veins, masses, and veinlets, and it is present mainly on the sides of interlayer faults and on the sides of orebodies in dolomitic limestone and dolomite.

Based on the composition, structure, framework, and strength of the altered rocks, combined with their spatial relationships with orebodies, the mineralization–alteration zones were delineated. From the orebodies to the wallrocks in the hanging wall, the mineralization–alteration zones of the C_2w Formation exhibit the following order: massive lead–zinc ore zone (I) → lead–zinc ore vein + pyrite vein zone + striped altered dolomite (Zone II) → striped altered dolomite zone (Zone III) → gray thick-layered dolomitic limestone zone (Zone IV). The mineralization–alteration zones of the D_3zg Formation exhibit the following order: massive lead–zinc ore + massive pyrite zone (Zone I) → lead–zinc ore vein + pyrite vein zone (Zone II) → spotted pyrite + dolomite vein zone (Zone III) → gray–white fine–medium crystalline dolomite zone (Zone IV). The detailed features and descriptions are shown in Figures 5–7; Table 1.

4.2 Porosity and permeability results for the two flanks of the anticline

For all the measured rock samples, the overall porosity and permeability changed greatly; the porosities ranged from 0.91% to 10.08%, and the permeabilities ranged from 0.003005251 – 17.68385095 × 10^{-3} μm^2 (Table 2).

The porosity–permeability scatter plot shows a positive correlation between the two flanks, and the slope (R) is 0.28827 ± 0.06658 (Figure 8).

The porosity of 1%–10.08% in the NW flank was greater than that of 0.91%–6.39% in the SE flank. The median value of the NW flank (2.74%) was greater than that of the SE flank (2.59%) (Figure 8).

The permeability of 0.003005251 – 17.68385095 × 10^{-3} μm^2 in the NW flank was greater than that of 0.003311688 – 0.723114436 × 10^{-3} μm^2 in the SE flank. In addition, the median value of the NW flank (0.01938 × 10^{-3} μm^2) was greater than that of the SE flank (0.0061 × 10^{-3} μm^2) (Figure 8).

4.3 Porosity and permeability results for the NW flank of the anticline

The porosities and permeabilities of rocks with different degrees of mineralization–alteration in the two main ore-bearing

10.3389/feart.2024.1347243

TABLE 1 Typical characteristics of the mineralization–alteration zones of different orebodies in the NW flank of the anticline.

Position	Orebody	Elevation (m)	Characteristic	Mineralization–alteration zones			
				Zone I	Zone II	Zone III	Zone IV
Hexi Hongjianshan ore block	H13	670	Mineralization–alteration	massive lead–zinc ore zone	lead–zinc ore vein + pyrite vein zone	striped altered dolomite zone	gray thick layered dolomitic limestone zone
			Minerals	galena + sphalerite + pyrite	galena + sphalerite + pyrite	dolomite	—
			Ore framework	euhedral, subhedral–xenomorphic granular	xenomorphic granular	xenomorphic granular	—
			Ore structure	massive	vein + mottled	striped	—
			Alteration	stronger	stronger	strong	weak
	H8	610	Mineralization–alteration	massive lead–zinc ore zone	lead–zinc veinlet +pyrite vein zone	striped altered dolomite + calcite veinlet zone	gray-white thick-layered dolomitic limestone zone
			Minerals	galena + sphalerite	galena + sphalerite + pyrite	dolomite + calcite	dolomite + calcite
			Ore framework	euhedral, subhedral–xenomorphic granular	subhedral–xenomorphic granular	xenomorphic granular	subhedral–xenomorphic
			Ore structure	massive	veinlet + vein + mottled	striped + veinlet	veinlet + veinlet
			Alteration	stronger	stronger	strong	weak
Hexi Qiancengdong ore block	Q1	755	Mineralization–alteration	vein lead–zinc zone	spotted pyrite + striped altered dolomite zone	striped altered dolomite zone	gray thick layered dolomitic limestone zone
			Minerals	galena + sphalerite	pyrite + dolomite	dolomite	dolomite + calcite
			Ore framework	euhedral–subhedral granular	subhedral–xenomorphic granular	xenomorphic granular	subhedral–xenomorphic
			Ore structure	vein	spotted + striped	striped	veinlet + veinlet
			Alteration	stronger	stronger	strong	weak
Hexi Shuilu ore block	S1	670	Mineralization–alteration	massive lead–zinc ore zone	lead–zinc veinlet + pyrite veinlet + striped altered dolomite zone	spotted pyrite + striped altered dolomite zone	gray thick layered dolomitic limestone zone
			Minerals	galena + sphalerite	galena + sphalerite + pyrite + dolomite	pyrite + dolomite	dolomite + calcite

(Continued on the following page)

10.3389/feart.2024.1347243

TABLE 1 (*Continued*)Typical characteristics of the mineralization–alteration zones of different orebodies in the NW flank of the anticline.

Position	Orebody	Elevation (m)	Characteristic	Mineralization–alteration zones			
				Zone I	Zone II	Zone III	Zone IV
			Ore framework	euhedral, subhedral–xenomorphic granular	subhedral–xenomorphic granular	xenomorphic granular	subhedral–xenomorphic
			Ore structure	massive	veinlet + disseminated + striped	spotted + striped	veinlet + veinlet
			Alteration	stronger	stronger	strong	weak
Hedong ore block	I–7	760	Mineralization–alteration	massive lead–zinc ore zone	vein lead–zinc + pyrite vein zone	spotted pyrite + dolomite vein zone	gray fine–medium crystalline fragmented dolomite zone
			Minerals	galena + sphalerite	galena + sphalerite + pyrite	pyrite + dolomite + calcite	dolomite + calcite
			Ore framework	euhedral–subhedral granular	subhedral–xenomorphic granular	xenomorphic granular	xenomorphic granular
			Ore structure	massive	vein	spotted + vein+ vein	veinlet + veinlet
			Alteration	stronger	stronger	strong	weaker
	I–6	683	Mineralization–alteration	massive lead–zinc ore + massive pyrite zone	lead–zinc vein + pyrite vein zone	spotted pyrite + dolomite vein zone	light-gray–gray–white fine–medium crystalline fragmented dolomite zone
			Minerals	galena + sphalerite + pyrite	galena + sphalerite + pyrite	pyrite + dolomite + calcite	calcite + dolomite
			Ore framework	euhedral–subhedral granular	subhedral–xenomorphic granular	xenomorphic granular	xenomorphic granular
			Ore structure	massive	vein	spotted + vein + vein	veinlet + mottled
			Alteration	stronger	strong	strong	weaker
	I–8	430	Mineralization–alteration	massive lead–zinc ore + massive pyrite zone	lead–zinc vein + massive pyrite zone	spotted pyrite + stockwork dolomite zone	gray–white fine–medium crystalline fragmented dolomite zone
			Minerals	galena + sphalerite + pyrite	galena + sphalerite + pyrite	pyrite + dolomite + calcite	dolomite + calcite
			Ore framework	euhedral–subhedral granular	subhedral–xenomorphic granular	xenomorphic granular	xenomorphic granular
			Ore structure	massive	vein + massive	spotted + stockwork + stockwork	veinlet + veinlet
			Alteration	stronger	stronger	strong	weaker

TABLE 2 Porosity and permeability results for different positions, different ore-bearing formations, and different alteration zones.

Anticline	Profile	Number	Formation	Lithology	Characteristic of mineralization–alteration	Diameter (cm)	Length (cm)	Volume (mL)	Input pressure (Kpa)	Flow (mL/min)	Porosity (%)	Permeability ($\times 10^{-3}$ um^2)
NW flank	The 32–33+1st line of 670 m of the H8 orebody in the Hexi Hongjianshan ore block	khwr–112	C_2w	gray fine–medium crystalline dolomitic limestone	mottled dolomite, a few fractures, fracture widths of 0.1–0.2 mm	2.513	2.974	0.527	301.7	24.8	3.57	0.640610773
		khwr–114	C_2w	gray fine crystalline limestone	a few vein dolomites, vein widths of 0.1–0.2 mm	2.502	5.011	0.463	312	3.35	1.88	0.139413601
	The 34+1st line of 610 m of the H8 orebody in the Hexi Hongjianshan ore block	khwr–121	C_2w	gray-white striped altered dolomite	many fractures, with widths of 0.1–0.2 mm	2.518	4.507	0.838	300.6	85.6	3.73	3.357080661
		khwr–122	C_2w	gray fine–medium crystalline dolomitic limestone	many vein coarse crystalline altered dolomite, vein widths of 1–10 mm	2.508	4.393	1.061	311.7	267.8	4.89	9.738586815
		khwr–123–1	C_2w	gray-white striped altered dolomite	medium vein lead–zinc, vein widths of 0.2–0.3 mm, a few fractures, fracture widths of 0.1–0.2 mm	2.474	4.963	0.423	301.6	46.8	1.78	2.082603347
		khwr–123–2	C_2w	gray-white striped altered dolomite	a few lead–zinc veins, vein widths of 0.1–0.2 mm, a few fractures, fracture widths of 0.1–0.2 mm	2.505	2.604	0.317	301.1	22.7	2.47	0.518339656
	khwr–125	C_2w	gray fine–medium crystalline dolomitic limestone	many vein coarse crystalline altered dolomite, vein widths of 1–10 mm	2.502	3.541	0.674	312	15.1	3.87	0.444057091	

(Continued on the following page)

TABLE 2 (*Continued*) Porosity and permeability results for different positions, different ore-bearing formations, and different alteration zones.

Anticline	Profile	Number	Formation	Lithology	Characteristic of mineralization–alteration	Diameter (cm)	Length (cm)	Volume (mL)	Input pressure (Kpa)	Flow (mL/min)	Porosity (%)	Permeability ($\times10^{-3}$ um^2)
		khwr–97	C_2w	gray fine–medium crystalline dolomitic limestone	mottled dolomite, a few pyrite veins, vein widths of 2–4 mm	2.508	3.672	0.453	306	0.195	2.5	0.006104795
	The 18th line of the 755 m of the Q1 orebody in the Hexi Qiancengdong ore block	khwr–98	C_2w	gray medium–coarse crystalline dolomitic limestone	spotted dolomite, spotted diameter of ~2 mm, a few fractures, fracture widths of 0.1–0.2 mm	2.539	3.24	0.741	305.1	2.9	4.52	0.078532151
		khwr–99	C_2w	gray-white striped altered dolomite	spotted pyrite, a few fractures, fracture widths of 0.1–0.2 mm	2.504	4.449	0.635	305	1.34	2.9	0.051257277
		khwr–100	C_2w	gray-white striped altered dolomite	mottled, medium vein lead–zinc, mottled diameter of ~10 mm, vein widths of 0.5–2 mm	2.508	2.417	0.304	304.4	0.16	2.55	0.003324776
		khwr–101	C_2w	gray fine–medium crystalline dolomitic limestone	medium vein dolomite, vein widths of 0.5–2 mm	2.478	5.012	0.426	306.8	2.61	1.76	0.113770033
		khwr–102	C_2w	gray fine–medium crystalline dolomitic limestone	a few vein dolomites, vein widths of 0.1–0.2 mm	2.5	4.097	0.521	312.1	0.3	2.59	0.010218684
		khwr–103	C_2w	gray-white striped altered dolomite	—	2.477	1.802	0.417	300.7	0.33	4.8	0.005344397

(Continued on the following page)

TABLE 2 (*Continued*) Porosity and permeability results for different positions, different ore-bearing formations, and different alteration zones.

Anticline	Profile	Number	Formation	Lithology	Characteristic of mineralization–alteration	Diameter (cm)	Length (cm)	Volume (mL)	Input pressure (Kpa)	Flow (mL/min)	Porosity (%)	Permeability ($\times 10^{-3}$ um^2)
	The 2nd line of the 670 m of the S1 orebody in the Hexi Shuilu ore block	khwr–141	C_2w	gray-white fine crystalline limestone	medium fractures, fracture widths of 0.2–0.5 mm	2.502	4.361	0.562	311	106	2.62	3.858859369
		khwr–143	C_2w	gray-white fine–medium crystalline dolomitic limestone	a few vein dolomites, vein widths of 0.2–0.5 mm, a few fractures, fracture widths of 0.1–0.2 mm	2.501	2.393	0.368	304.1	2.5	3.13	0.051803484
		khwr–145	C_2w	gray-white medium–coarse crystalline dolomitic limestone	spotted dolomite, pyrite, spotted diameter of ~5 mm, a few fractures, fracture widths of 0.1–0.2 mm	2.442	4.674	1.137	301.6	0.45	5.19	0.019356451
		khwr–147	C_2w	gray-white fine–medium crystalline dolomitic limestone	medium vein dolomite, vein widths of 2–5 mm, many fractures, fracture widths of 0.1–0.2 mm	2.473	3.709	0.523	302.4	8.6	2.93	0.285030043
	The 116th line of the 760 m of the I-7 orebody in the Hedong ore block	khwr–42	D_3zg^{3-2}	gray-white medium–coarse crystalline dolomite	a few lead–zinc veins, calcite, vein widths of 10–15 mm	2.503	3.474	0.652	310.8	0.345	3.81	0.010007273
		khwr–43	D_3zg^{3-2}	massive pyrite ore	—	2.502	4.999	0.591	312.1	0.26	2.41	0.010788713
		khwr–45	D_3zg^{3-2}	gray-white medium–coarse crystalline dolomite	disseminated pyrite	2.506	2.13	0.399	311.6	0.29	3.8	0.005124101
		khwr–46	D_3zg^{3-2}	gray-white medium–coarse crystalline dolomite	mottled lead–zinc, mottled diameter of ~50 mm, a few fractures, fracture widths of 0.1–0.2 mm	2.503	2.996	0.441	311.8	0.43	2.99	0.010701505

(Continued on the following page)

TABLE 2 (*Continued*) Porosity and permeability results for different positions, different ore-bearing formations, and different alteration zones.

Anticline	Profile	Number	Formation	Lithology	Characteristic of mineralization–alteration	Diameter (cm)	Length (cm)	Volume (mL)	Input pressure (Kpa)	Flow (mL/min)	Porosity (%)	Permeability ($\times10^{-3}$ um^2)
	The 98+1st line of the 683 m of the I-6 orebody in the Hedong ore block	khwr–51	D_3zg^{3-2}	gray-white fine–medium crystalline dolomite	—	2.506	4.985	0.451	312	0.09	1.83	0.003714121
		khwr–52	D_3zg^{3-2}	massive pyrite ore	a few fractures, fracture widths of 0.1–0.2 mm	2.5	2.059	1.019	311.1	68.5	10.08	1.178650735
		khwr–53	D_3zg^{3-2}	massive lead–zinc ore	a few fractures, fracture widths of 1–2 mm	2.5	4.046	0.57	311.3	261.7	2.87	8.839368463
		khwr–54–1	D_3zg^{3-2}	gray-white coarse crystalline dolomite	mottled dolomite, stockwork pyrite, vein widths of 2–5 mm, a few fractures, fracture widths of 1–2 mm	2.499	3.318	0.794	310.7	154.2	4.88	4.287857634
		khwr–54–2	D_3zg^{3-2}	gray-white fine–medium crystalline dolomite	mottled dolomite	2.504	4.993	0.41	312.1	0.088	1.67	0.003641358
		khwr–56	D_3zg^{3-2}	gray-white fine–medium crystalline dolomite	mottled calcite	2.503	3.506	0.494	311.5	0.19	2.86	0.005542033
		khwr–57	D_3zg^{3-2}	gray-white brecciated dolomite	adhesive stockwork calcite, vein widths of 1–5 mm	2.504	4.987	1.005	31.4	9.17	4.09	7.850477067
	The 92nd line of the 670 m in the Hedong ore block	khwr–61	D_3zg^{3-2}	dark gray fine crystalline dolomite	a few fractures, fracture widths of 0.5–1 mm	2.523	4.123	0.407	308.2	0.92	1.97	0.031592771
		khwr–64	D_3zg^{3-2}	gray fine–medium crystalline dolomite	spotted dolomite, spotted diameter of ~5 mm, rice-grain texture	2.5	4.98	1.054	310.7	0.13	4.31	0.005421317

(Continued on the following page)

TABLE 2 (*Continued*) Porosity and permeability results for different positions, different ore-bearing formations, and different alteration zones.

Anticline	Profile	Number	Formation	Lithology	Characteristic of mineralization–alteration	Diameter (cm)	Length (cm)	Volume (mL)	Input pressure (Kpa)	Flow (mL/min)	Porosity (%)	Permeability ($\times10^{-3}$ um^2)
		khwr–65	D_3zg^{3-2}	gray fine–medium crystalline dolomite	a few vein dolomites, vein widths of 0.3–0.5 mm, fractures in vertical core	2.501	3.475	0.48	311.8	0.19	2.81	0.00549335
		khwr–68	D_3zg^{3-2}	gray-white fine–medium crystalline dolomite	a few vein dolomites, vein widths of 1–2 mm, fractures in vertical core	2.502	3.297	0.344	309.8	0.15	2.12	0.004153962
		khwr–70	D_3zg^{3-2}	gray-white fine–medium crystalline dolomite	—	2.504	4.993	0.342	311.5	0.195	1.39	0.008093807
	The 96–112nd line of the 610 m of the I-6 orebody in the Hedong ore block	khwr–71	D_3zg^{3-2}	gray fine crystalline dolomite	a few vein calcites, vein widths of 0.1–2 mm	2.499	4.991	0.455	312.4	0.33	1.86	0.013683236
		khwr–72	D_3zg^{3-2}	gray fine crystalline dolomite	medium vein calcite, vein widths of 1–10 mm	2.505	4.979	0.503	312.6	0.8	2.05	0.032899664
		khwr–73	D_3zg^{3-2}	gray fine crystalline dolomite		2.501	4.397	0.543	312.2	0.13	2.51	0.004746107
		khwr–76	D_3zg^{3-2}	gray-white fine–medium crystalline dolomite	Stockwork calcite, vein widths of 0.2–5 mm	2.503	2.683	0.76	311.6	274.3	5.75	6.119656209
	The stope of the 490 m of the I-8 orebody in the Hedong ore block	khwr–83	D_3zg^{3-2}	gray fine crystalline dolomite	a few fractures, fracture widths of 0.1–0.2 mm	2.527	3.486	0.443	309.2	9	2.54	0.259138707
		khwr–85	D_3zg^{3-2}	gray fine crystalline dolomite	Stockwork dolomite, vein widths of 1–5 mm	2.498	4.069	0.699	305.7	504.9	3.5	17.68385095

(Continued on the following page)

10.3389/feart.2024.1347243

TABLE 2 (*Continued*) Porosity and permeability results for different positions, different ore-bearing formations, and different alteration zones.

Anticline	Profile	Number	Formation	Lithology	Characteristic of mineralization–alteration	Diameter (cm)	Length (cm)	Volume (mL)	Input pressure (Kpa)	Flow (mL/min)	Porosity (%)	Permeability ($\times 10^{-3} um^2$)
	The stope of the 430 m of the I-8 orebody in the Hedong ore block	khwr–31	D_3zg^{3-2}	gray-white fine crystalline dolomite	a few fractures, fracture widths of 0.1–0.5 mm	2.504	2.853	0.306	307.2	0.8	2.18	0.019399858
		khwr–32	D_3zg^{3-2}	massive pyrite ore	—	2.502	2.939	0.813	311.3	6.64	5.63	0.162653985
		khwr–33	D_3zg^{3-2}	massive lead–zinc ore	hole development, hole width of ~2 mm	2.502	2.639	1.013	310.6	54.9	7.81	1.211916955
	The 90–96th line of the 370 m of the I-8 orebody in the Hedong ore block	khwr–22	D_3zg^{3-2}	gray-white fine crystalline dolomite	medium fractures, fracture widths of 0.1–0.2 mm	2.451	2.502	0.277	308.5	93.3	2.34	2.056971567
		khwr–23	D_3zg^{3-2}	gray-white fine–medium crystalline dolomite	a few fractures, fracture widths of 0.1–0.2 mm	2.476	2.751	0.447	320.7	1.24	3.38	0.027679793
		khwr–25	D_3zg^{3-2}	gray-white coarse crystalline dolomite	a few fractures, fracture widths of 0.1–0.2 mm	2.504	2.691	0.588	318.6	0.52	4.43	0.011219772
	The 98–104th line of the 310 m of the I-8 orebody in the Hedong ore block	khwr–2	D_3zg^{3-2}	gray-white medium–coarse crystalline dolomite	a few vein dolomites, vein widths of 1–2 mm	2.499	3.142	0.819	312	0.62	5.31	0.016217201
		khwr–4	D_3zg^{3-2}	gray-white medium–coarse crystalline dolomite	mottled pyrite, a few vein dolomites, vein widths of 1–3 mm	2.498	4.24	0.774	312.4	0.96	3.73	0.033843248
		khwr–12	D_3zg^{3-2}	gray-white coarse crystalline dolomite	spotted dolomite, spotted diameter of ~2 mm, a few dolomite veins, vein widths of 1–2 mm	2.522	1.96	0.578	307.7	1.03	5.9	0.01687138

(Continued on the following page)

TABLE 2 (*Continued*) Porosity and permeability results for different positions, different ore-bearing formations, and different alteration zones.

Anticline	Profile	Number	Formation	Lithology	Characteristic of mineralization–alteration	Diameter (cm)	Length (cm)	Volume (mL)	Input pressure (Kpa)	Flow (mL/min)	Porosity (%)	Permeability ($\times10^{-3}um^2$)
	Surface	HX–115	P_2q+m	gray fine crystalline limestone	mottled, medium vein calcite, mottled diameter of ~10 mm, vein widths of 0.2–2 mm	2.504	5.005	0.558	311.6	0.53	2.26	0.022040099
		HX–116	P_2q+m	gray fine crystalline limestone	—	2.498	4.976	0.369	312	0.16	1.51	0.006633245
		HD–114	P_2q+m	dark gray fine crystalline limestone	vein coarse crystalline dolomite, vein widths of 5–6 mm, medium vein calcite, vein widths of 1–3 mm	2.498	4.994	0.891	310.2	15.2	3.64	0.63831948
		HD–115	P_2q+m	dark gray fine crystalline limestone	—	2.5	4.999	0.363	310.4	0.19	1.48	0.007965992
		HX–112	C_2w^{1-3}	gray-white fine crystalline dolomitic limestone	—	2.496	5.003	0.336	310	0.14	1.37	0.005905384
		HX–113	C_2w^2	gray-white fine crystalline dolomitic limestone	a few fractures, fracture widths of 0.2–1 mm	2.5	5	0.507	311.4	0.48	2.07	0.02002533
		HX–114	C_2w^2	gray-white coarse crystalline dolomite	—	2.499	5	0.459	312.2	0.155	1.87	0.006445168
		HD–108	C_2w^{1-2}	gray-yellow medium–coarse crystalline dolomite	many fractures, fracture widths of 0.5–1 mm, fractures filled with yellow-brown iron-rich mud material	2.497	4.988	1.475	310.5	3.45	6.04	0.144599861

(Continued on the following page)

10.3389/feart.2024.1347243

TABLE 2 (*Continued*) Porosity and permeability results for different positions, different ore-bearing formations, and different alteration zones.

Anticline	Profile	Number	Formation	Lithology	Characteristic of mineralization–alteration	Diameter (cm)	Length (cm)	Volume (mL)	Input pressure (Kpa)	Flow (mL/min)	Porosity (%)	Permeability ($\times10^{-3}um^2$)
		HD–109	C_2w^{1-1}	gray-white fine crystalline dolomitic limestone	spotted dolomite, spotted diameter of ~2 mm, a few dolomite veins, vein widths of 0.5–1 mm	2.499	5	0.33	310	3.65	1.34	0.15350026
		HD–110	C_2w^{1-3}	gray-white fine crystalline dolomitic limestone	—	2.499	5.005	0.292	310	0.085	1.19	0.003578238
		HD–111	C_2w^{1-3}	gray-white fine crystalline dolomitic limestone	mottled dolomite	2.497	5.006	0.609	310	0.158	2.49	0.006663304
		HD–112	C_2w^2	gray-white fine crystalline dolomitic limestone	—	2.497	4.999	0.315	310	0.105	1.29	0.004421953
		HD–113	C_2w^2	gray-white fine crystalline dolomitic limestone	—	2.495	5.002	0.321	310.3	0.16	1.31	0.006742633
		HX–9	C_1d^1	dark gray sparite limestone	—	2.5	4.994	0.246	305.6	0.08	1	0.003435215
		HX–10	C_1d^1	gray-white quartz sandstone	stockwork fractures, fracture widths of 0.5–1 mm, fractures filled with yellow-brown iron-rich mud material	2.503	3.308	0.987	303.8	317	6.07	9.080088277

(Continued on the following page)

10.3389/feart.2024.1347243

TABLE 2 (*Continued*) Porosity and permeability results for different positions, different ore-bearing formations, and different alteration zones.

Anticline	Profile	Number	Formation	Lithology	Characteristic of mineralization–alteration	Diameter (cm)	Length (cm)	Volume (mL)	Input pressure (Kpa)	Flow (mL/min)	Porosity (%)	Permeability ($\times 10^{-3} um^2$)
		HX–11	C_1d^2	dark gray fine crystalline limestone	a few fractures, fracture widths of 0.2–0.5 mm	2.502	4.058	0.723	304.7	8.25	3.63	0.288755333
		HX–108	C_1d^1	gray fine crystalline limestone	—	2.498	5.006	0.411	307.7	0.13	1.67	0.005543663
		HX–109	C_1d^2	gray fine crystalline limestone	stockwork calcite, vein widths of 0.1–5 mm	2.5	5	1.021	308.8	0.97	4.16	0.041014095
		HX–110	C_1d^3	gray–white fine crystalline limestone	—	2.499	4.986	0.483	300.6	0.13	1.97	0.005726312
		HX–111	C_1b	gray–white dolomitic limestone	—	2.507	4.994	0.462	308.8	0.17	1.87	0.007139375
		HX–101	D_3zg^{3-1}	gray–white fine crystalline dolomite	hole development, hole width of ~1 mm, a few fractures, fracture widths of 1–2 mm, fractures filled with yellow–brown iron-rich mud material	2.495	4.998	0.4	304.9	0.25	1.64	0.010826281
		HX–102	D_3zg^{3-1}	gray–white fine crystalline dolomite	medium fractures, fracture widths of 1–2 mm	2.5	4.986	0.654	304.4	56.1	2.67	2.420226284
		HX–103	D_3zg^{3-1}	gray–white medium–coarse crystalline dolomite	hole development, hole diameter of ~1 mm, a few calcite veins, vein widths of 0.5–1 mm	2.499	3.16	0.64	304.3	14.6	4.13	0.399719941
		HX–104	D_3zg^{3-1}	gray brecciated dolomite	adhesive stockwork calcite, vein widths of 2–5 mm	2.501	4.993	1.164	305.5	2.74	4.75	0.117599884

(Continued on the following page)

10.3389/feart.2024.1347243

TABLE 2 (*Continued*) Porosity and permeability results for different positions, different ore-bearing formations, and different alteration zones.

Anticline	Profile	Number	Formation	Lithology	Characteristic of mineralization–alteration	Diameter (cm)	Length (cm)	Volume (mL)	Input pressure (Kpa)	Flow (mL/min)	Porosity (%)	Permeability ($\times 10^{-3} um^2$)
		HX–105	D_3zg^{3-1}	gray–white fine crystalline dolomite	hole development, hole diameter of ~2 mm, medium fractures, fracture widths of 0.5–1 mm	2.495	4.987	0.609	305.4	0.85	2.5	0.036632468
		HX–106	D_3zg^{3-2}	light-gray coarse crystalline dolomite	mottled calcite, hole development, hole diameter of ~2 mm, many fractures, fracture widths of 1–2 mm, fractures filled with yellow-brown iron-rich mud material	2.497	5.003	0.764	304.6	23	3.12	0.996981802
		HX–1	D_3zg^{3-2}	gray-white medium–coarse crystalline dolomite	hole development, hole diameter of ~2 mm, a few fractures, fracture widths of 0.5–1 mm	2.506	4.057	0.784	302.5	0.29	3.92	0.010232829
		HX–2	D_3zg^{3-2}	gray fine crystalline dolomite	—	2.503	4.992	0.269	305.1	0.07	1.09	0.003005251
		HX–3	D_3zg^{3-2}	gray fine crystalline dolomite	hole development, hole diameter of ~10 mm, holes filled with yellow-brown iron-rich mud material, medium fractures, fracture widths of 5–6 mm, fractures filled with yellow-brown iron-rich mud material	2.502	4.988	0.708	304.3	0.25	2.89	0.010778051

(Continued on the following page)

TABLE 2 (*Continued*) Porosity and permeability results for different positions, different ore-bearing formations, and different alteration zones.

Anticline	Profile	Number	Formation	Lithology	Characteristic of mineralization–alteration	Diameter (cm)	Length (cm)	Volume (mL)	Input pressure (Kpa)	Flow (mL/min)	Porosity (%)	Permeability ($\times10^{-3}um^2$)
		HX-4-5	D_3zg^{3-2}	gray-white fine crystalline dolomite	many vein coarse crystalline dolomites, vein widths of 5–6 mm, hole development, hole diameter of ~10 mm, holes filled with yellow-brown iron-rich mud material	2.502	4.975	1.467	305.3	0.18	6	0.007699577
		HX-4-4	D_3zg^{3-2}	gray-white fine crystalline dolomite	—	2.501	4.995	0.586	305.1	0.08	2.39	0.003442136
		HX-4-1	D_3zg^{3-2}	gray-white fine crystalline dolomite	—	2.502	5.007	0.538	305.5	0.09	2.18	0.003870505
		HX-4-2	D_3zg^{3-2}	gray-white fine crystalline dolomite	a few vein coarse crystalline dolomites, vein widths of 5–6 mm, hole development, hole diameter of ~5 mm, holes filled with yellow-brown iron-rich mud material	2.507	4.998	0.902	305.4	0.22	3.65	0.009411509
		HX-4-3	D_3zg^{3-2}	gray-white fine crystalline dolomite	—	2.5	4.993	0.404	305.8	0.1	1.65	0.004288679
		HX-6	D_3zg^{3-3}	gray-white fine crystalline dolomite	—	2.506	4.985	0.575	305.5	0.08	2.34	0.003414406

(Continued on the following page)

TABLE 2 (*Continued*) Porosity and permeability results for different positions, different ore-bearing formations, and different alteration zones.

Anticline	Profile	Number	Formation	Lithology	Characteristic of mineralization–alteration	Diameter (cm)	Length (cm)	Volume (mL)	Input pressure (Kpa)	Flow (mL/min)	Porosity (%)	Permeability ($\times10^{-3}um^2$)
		HX–7	D_3zg^{3-3}	gray–white medium–coarse crystalline dolomite	a few fractures, fracture widths of 1–2 mm	2.505	4.995	0.877	305.2	1	3.56	0.04286698
		HX–8	D_3zg^{3-3}	gray–white medium–coarse crystalline dolomite	hole development, hole diameters of 1–2 mm, a few fractures, fracture widths of 0.1–0.2 mm	2.502	4.986	0.916	304.9	0.9	3.74	0.03866378
SE flank	Surface	HD–1	P_2q+m	gray fine crystalline limestone	—	2.495	5.001	0.225	307.2	0.1	0.92	0.004281453
		HD–2	P_2q+m	gray fine crystalline limestone	—	2.498	5.003	0.261	312.4	0.1	1.06	0.004159733
		HD–3	C_2w^2	gray fine crystalline limestone	—	2.497	5	0.222	312.2	0.085	0.91	0.003540111
		HD–4	C_2w^2	gray fine crystalline limestone	—	2.5	4.997	0.274	312.8	0.08	1.12	0.003311688
		HD–5	C_2w^2	gray fine crystalline limestone	—	2.498	5.003	0.295	311.9	0.09	1.2	0.003753371
		HD–6	C_2w^2	red-brown brecciated limestone	adhesive mottled yellow–brown iron-rich mud material	2.505	4.989	0.883	312	0.09	3.59	0.00372007
		HD–8	C_2w^{1-3}	gray fine crystalline limestone	a few fractures, fracture widths of 0.1–1 mm, fractures in vertical core, yellow–brown iron-rich mud filling	2.505	5.004	0.489	312	0.14	1.98	0.005804174

(Continued on the following page)

10.3389/feart.2024.1347243

TABLE 2 (*Continued*) Porosity and permeability results for different positions, different ore-bearing formations, and different alteration zones.

Anticline	Profile	Number	Formation	Lithology	Characteristic of mineralization–alteration	Diameter (cm)	Length (cm)	Volume (mL)	Input pressure (Kpa)	Flow (mL/min)	Porosity (%)	Permeability ($\times10^{-3}um^2$)
		HD–9	C_2w^{1-3}	gray fine crystalline limestone	—	2.501	2.494	0.29	312	0.295	2.37	0.006115073
		HD–11	C_2w^{1-2}	gray fine crystalline limestone	a few vein coarse crystalline dolomites, vein widths of 1–2 mm	2.5	3.884	0.665	310	0.187	3.49	0.006104071
		HD–13	C_2w^{1-2}	gray fine crystalline limestone	—	2.501	4.99	0.314	309.3	0.1	1.28	0.004205538
		HD–15	C_2w^{1-1}	gray-white, red-brown coarse crystalline dolomite	a few fractures, fracture widths of 1–2 mm	2.5	4.993	1.567	311	2.75	6.39	0.114803691
		HD–16	C_1b	red-brown coarse crystalline dolomite	vein calcite, vein widths of 2–6 mm	2.502	4.984	0.847	310.6	0.85	3.45	0.035437093
		HD–17	C_1b	gray-white, red-brown brecciated limestone	adhesive red-brown iron-rich mud material	2.503	4.994	1.193	310	0.24	4.86	0.010048861
		HD–19	C_1d^3	gray brecciated limestone	adhesive mottled yellow-brown iron-rich mud material, medium vein coarse crystalline dolomite, vein widths of 5–6 mm	2.498	4.985	1.14	310.5	0.126	4.66	0.005273637
		HD–101	D_3zg^{3-3}	gray brecciated dolomite	hole development, hole diameter of ~1 mm, stockwork dolomite, vein widths of 1–5 mm	2.498	4.985	0.924	310	0.86	3.78	0.036087559

(Continued on the following page)

10.3389/feart.2024.1347243

TABLE 2 (*Continued*) Porosity and permeability results for different positions, different ore-bearing formations, and different alteration zones.

Anticline	Profile	Number	Formation	Lithology	Characteristic of mineralization–alteration	Diameter (cm)	Length (cm)	Volume (mL)	Input pressure (Kpa)	Flow (mL/min)	Porosity (%)	Permeability ($\times10^{-3}um^2$)
		HD–102	D_3zg^{3-3}	gray fine crystalline dolomite	—	2.501	4.997	0.636	311.6	0.23	2.59	0.009572206
		HD–103	D_3zg^{3-3}	gray brecciated dolomite	hole development, hole diameter of ~2 mm, stockwork dolomite, vein widths of 3–5 mm	2.498	4.987	0.886	310	0.34	3.63	0.014272898
		HD–104	D_3zg^{3-2}	gray fine crystalline dolomite	—	2.499	4.996	0.514	309	0.173	2.1	0.007307319
		HD–105	D_3zg^{3-1}	gray brecciated dolomite	hole development, hole diameter of ~2 mm, medium vein dolomite, vein widths of 1–5 mm	2.504	4.99	1.184	308.9	17.2	4.82	0.723114436

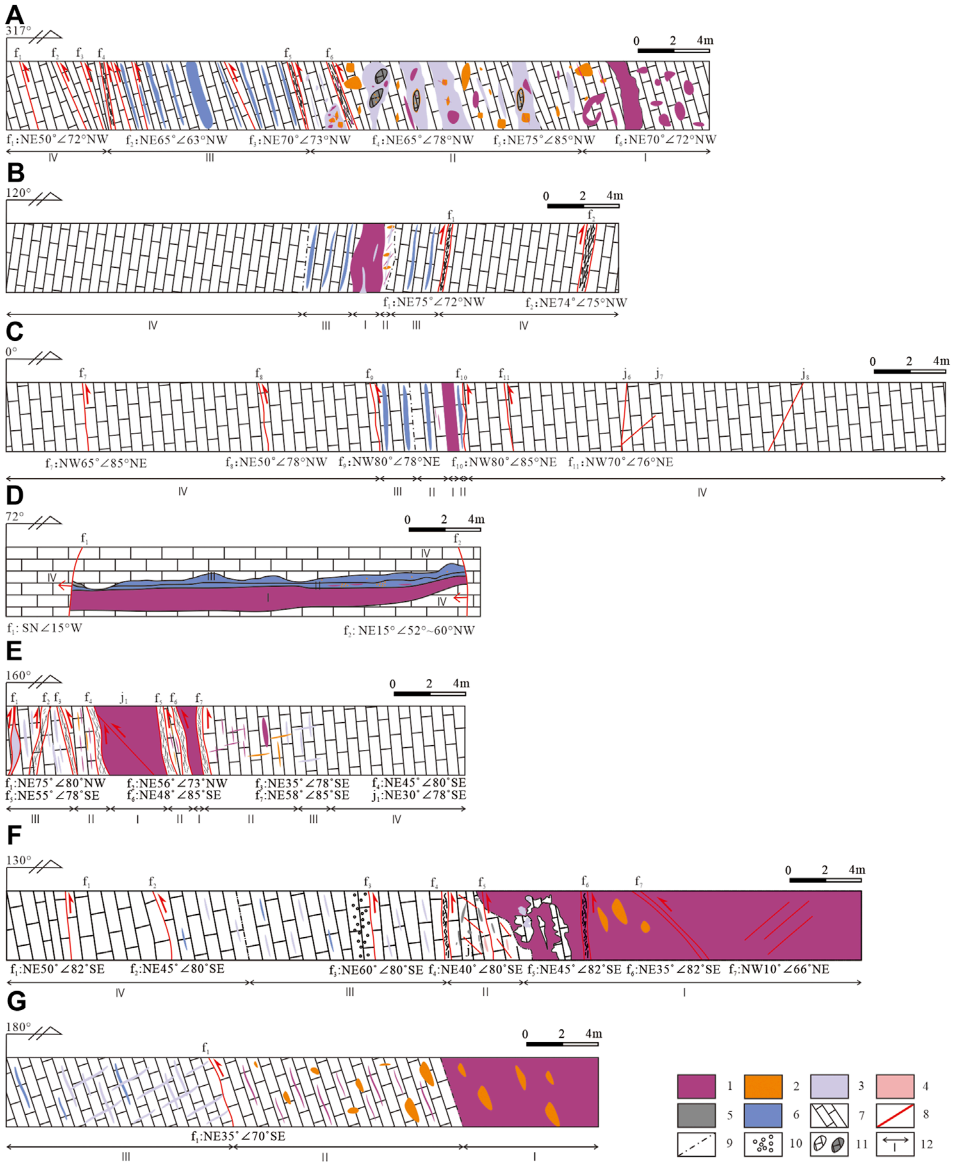

FIGURE 5
Typical mineralization–alteration zones geological profile of Maoping lead–zinc deposit. The expression of fault occurrence is: trend∠dip–direction. 1—Orebody; 2—Pyrite; 3—Calcite; 4—Sphalerite; 5—Galena; 6—Dolomite; 7—Formation; 8—Fault; 9—Alteration boundary; 10—Corrosion hole; 11—Wall-rock breccia; 12—Alteration zoning. **(A)**—the 32–33+1st line of 670 m of the H8 orebody in the Hexi Hongjianshan ore block; **(B)**—the 34+1st line of 610 m of the H8 orebody in the Hexi Hongjianshan ore block; **(C)**—the 18th line of the 755 m of the Q1 orebody in the Hexi Qiancengdong ore block; **(D)**—the 2nd line of the 670 m of the S1 orebody in the Hexi Shuilu ore block; **(E)**—the 116th line of the 760 m of the I-7 orebody in the Hedong ore block; **(F)**—the 98+1st line of the 683 m of the I-6 orebody in the Hedong ore block; **(G)**—the stope of the 430 m of the I-8 orebody in the Hedong ore block.

formations (C_2w and D_3zg) on the NW flank of the anticline were analyzed (Figure 9).

The porosity results show that in the C_2w Formation, the percentage of unaltered rock (1.19%–2.62%; median value: 1.87%) is the lowest, followed by the orebody (1.78%–2.90%; median value: 2.51%), and the highest percentage of dolomitized rock (2.93%–5.19%; median value: 3.87%). The porosity results show that in the D_3zg Formation, the percentage of unaltered rock (1.09%–2.39%; median value: 1.83%) is the lowest, followed by dolomitized rock (3.12%–5.90%; median value: 4.31%), and the highest percentage of orebody rock (2.87%–10.08%; median value: 5.26%).

The permeability results show that for both the C_2w and D_3zg Formations, the permeability also decreases with decreasing erosion. In the C_2w Formation, the median

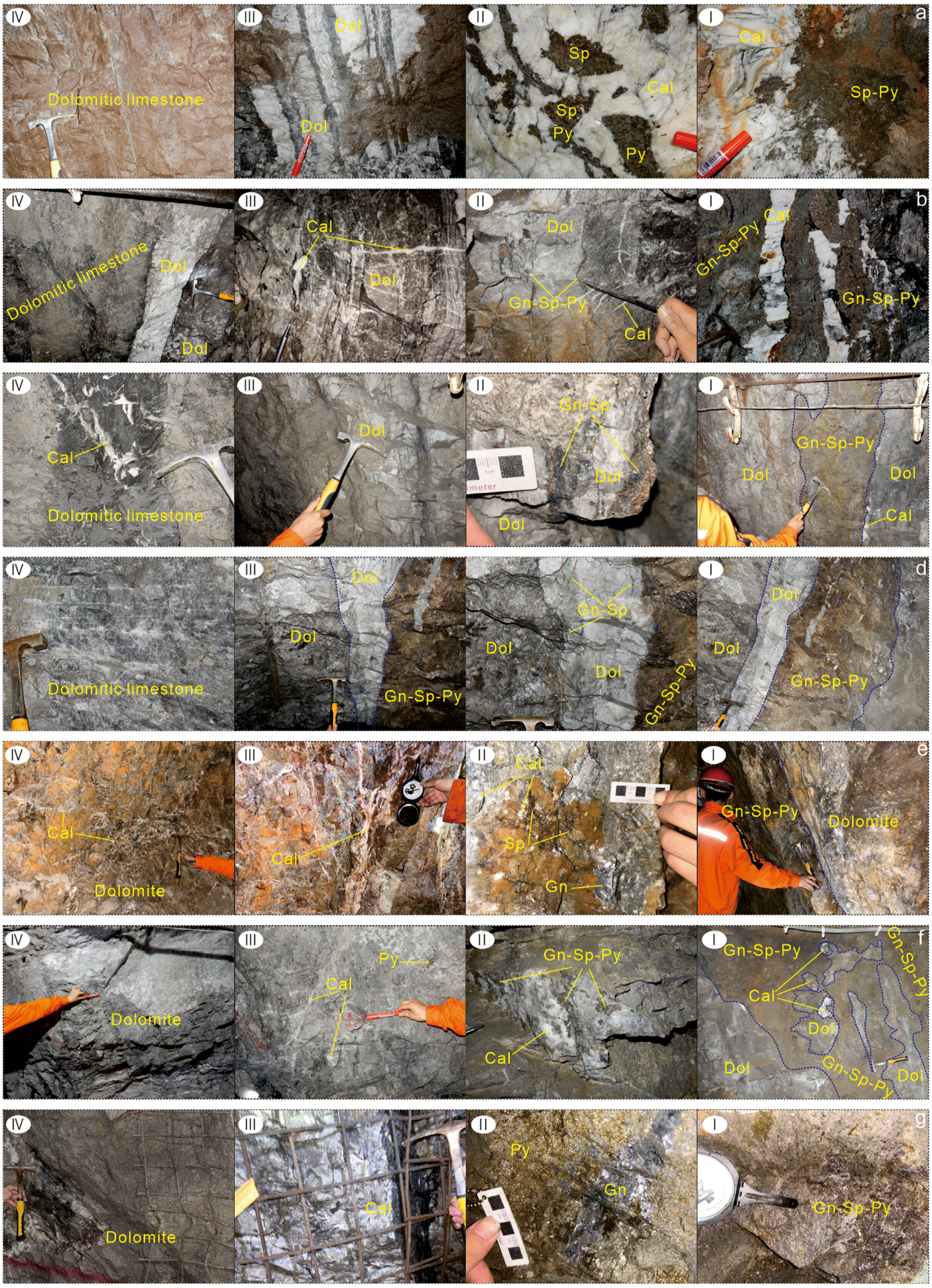

FIGURE 6
Geological profile of Maoping lead–zinc deposit mineralization–alteration zones field macroscopic characteristics. **(A, B)** is the same as Figure 4; I-IV represents various mineralization–alteration zones.

values of strong alteration, moderate alteration, weak alteration, and no alteration are 3.608, 0.219, 0.036 and 0.006, respectively; in the D_3zg Formation, the median values of strong alteration, moderate alteration, weak alteration, and no alteration are 4.288, 0.259, 0.017 and 0.005, respectively.

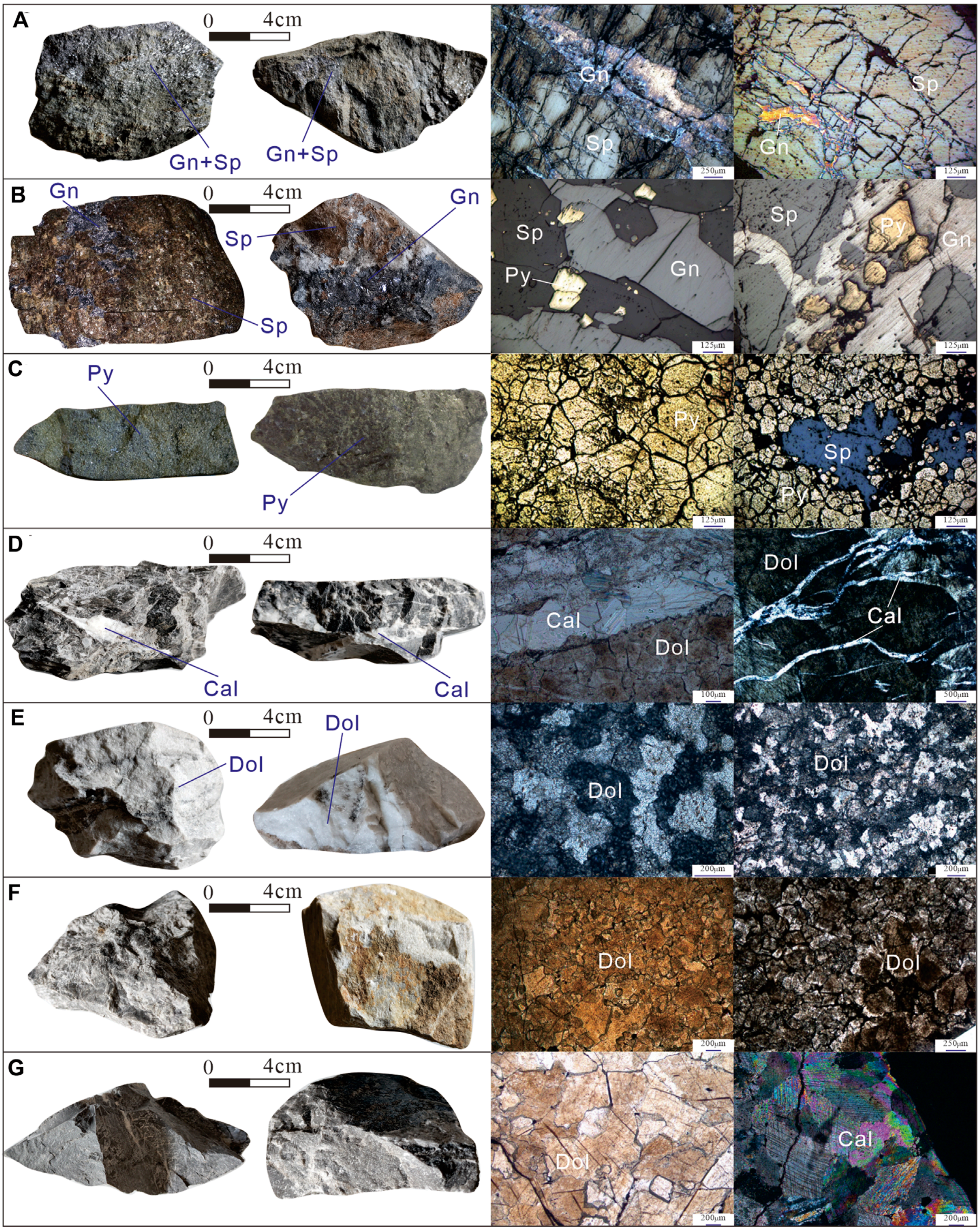

FIGURE 7
Typical mineralization–alteration samples of the Maoping lead–zinc deposit and their microscopic and Macroscopic characteristics. **(A)**—Massive lead–zinc ore in dolomite of D_3zg formation, **(B)**—Massive lead–zinc ore in dolomite of C_2w formation; **(C)**—Massive pyrite, **(D)**—vein calcite, **(E)**—Striped altered dolomite zone, **(F)**—Unaltered dolomite, **(G)**—Unaltered dolomitic limestone.

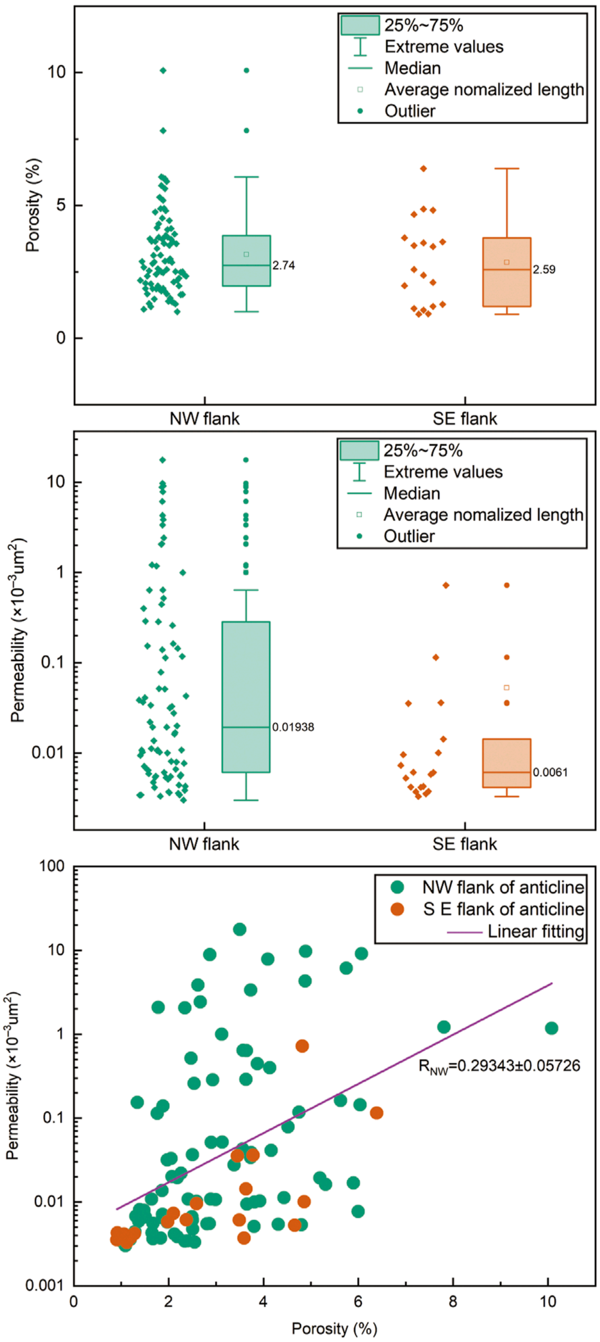

FIGURE 8
Distribution and correlation maps of porosity and permeability on the two flanks of the anticline.

5 Discussion

5.1 The geological significance of porosity and permeability

The fault in this study is a complex four-dimensional tectonic unit composed of a fault surface and tectonite, and its tectonic deformation and fluid flow characteristics evolve over time Wibberley and Shipton. (2010). Tectonics are not only the dominant factor controlling the coupling relationship between geological bodies but also the main driving force for fluid migration; various tectonic features, such as faults, fractures, and breccia zones, provide channels for fluid migration in the subsurface (Zhai, 1996). These features can also enhance permeability, hydraulic conductivity, and hydrothermal flow, thereby increasing the mineralization potential of favorable sedimentary locations (Henderson and McCaig, 1996; Cox et al., 2001; Bauer et al., 2022). The degree of rock fragmentation, permeability, local porosity and fluid flux are different in different parts where tectonic deformation occurs (such as bends and branches of fracture zones), which leads to different mineralization types and mineralization intensities (Soden et al., 2014; Zhang, 2017).

Fluids can control the deformation process of rocks and even alter the deformation mechanism of rocks through physical changes or chemical reactions, such as hydrolysis weakening and reducing the friction coefficient between mineral particles Wintsch et al. (1995). The dissolution and precipitation of minerals during water-rock reactions can cause changes in fluid composition and affect rock properties (Wawrzyniec, 1999). The properties of the fluid are the main factors controlling microprocesses, such as the generation of cementitious materials, pore characteristics, and mineral precipitation in the host rock (Wu et al., 2015). Carbonate minerals not only metasomatically fill pores but also dolomitize and recrystallize in limestone and dolomite (Corbella et al., 2004), forming medium–coarse-grained altered dolomite, allomorphic granular mineral particles at the microscale, and calcite veins, dolomite veins, and pyrite veins, thus increasing the porosity and permeability.

Tectonic action affects the properties, migration, and precipitation of fluids, thereby controlling the alteration characteristics generated during fluid migration and changing the porosity and permeability. Different types and degrees of alteration have different porosities and permeabilities (Figures 8, 9).

Research has shown that, overall, the NW flank of the Maomaoshan anticline has greater porosities and permeabilities than the SE flank (Figure 8). The strata in the NW flank of the Maomaoshan anticline are steeply inclined and inverted (with dip angles of 55°–85°), while those in the SE flank are gently inclined (with dip angles of 20°–35°). The orebody in this deposit is controlled by interlayer faults. Under the action of tectonic forces, when the local principal compressive stress directions on both flanks are consistent, the strata in the NW flank have a large dip angle, and the compressive surface of the NW flank exhibits mainly compressive stress, as well as shear resistance. The strata in the SE flank have a small dip angle, and the compressive surface of the SE flank exhibits mainly shear resistance, followed by tensile resistance. When relative sliding occurs in interlayer faults, they are affected not only by the principal compressive stress but also by the gravity of the rock or the block itself. Both the NW flank and SE flank interlayer faults are known to have experienced relative motion. For the same rock formation, the compressive strength is generally greater than the shear strength, making it more prone to shear deformation. Therefore, the SE flank

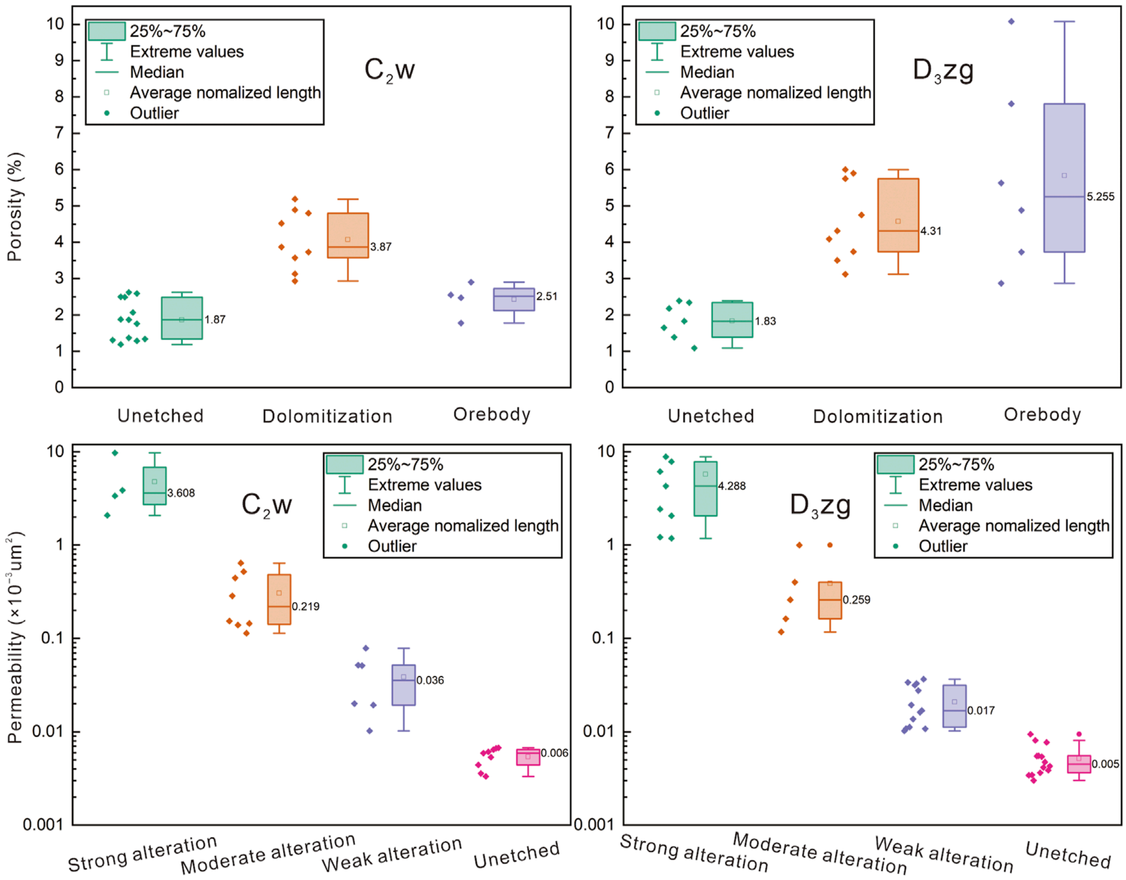

FIGURE 9
Porosity and permeability characteristics of different types and intensities with mineralization–alteration in NW flank of the anticline.

can achieve only the minimum force required for shear resistance before relative sliding occurs, resulting in compressional–torsional faulting and stress release. The NW flank achieves not only the minimum force required for shear resistance but also the minimum force required for rock compression resistance. Not only does relative sliding occur, but it also causes damage to the rock, forming an open space. This is more conducive to fluid "penetration".

Therefore, the NW flank of the anticline is more conducive to mineralization.

5.2 Metallogenic patterns and prospecting directions

During the mineralization period, the ore-forming fluid migrated upward along the main ore-guiding structure (NE-trending Maoping sinistral compressive–torsional fault) and generally migrated from deep in the SSW region to shallow in the NNE region. Through the ore distribution structure (SN-trending Luozehe sinistral torsional fault, NE-trending Maomaoshan compound overturned anticline, NNW-trending sinistral torsional–extensional fault, and NE-trending subsequent compressional–torsional fault), the fluid reached the NE-trending interlayered sinistral compressive–torsional faults (Figure 10) (Wu et al., 2023), and hydrothermal "penetration" metasomatism occurred.

Due to the effect of the overlying clastic rock barrier, when deep-source fluids rich in Pb^{2+}, Zn^{2+}, and Ge^{2+} and other cations and basin fluids rich in reduced sulfur entered the expansion space, boiling decompression occurred in the overlying host carbonate bed under the barrier layer, and the pH increased, resulting in mineral precipitation. The medium–coarse-grained altered dolomite that formed in the early stage of fluid interaction was conducive to further water–rock interactions between the fluid and the surrounding rock, leading to the precipitation of lead and zinc minerals (acid generation) and the mutual promotion of wallrock alteration (acid consumption) (Zhang et al., 2016; Ali et al., 2017; Korges et al., 2018; Zhang et al., 2019), thus forming a zone of brecciated hot-solution dolomite lead–zinc mineralization (Figure 10).

The striped altered dolomite zone (Zones II–III) in the C_2w limestone and the pyritization + strong dolomitization zone (Zones II–III) in the D_3zg dolomite are important prospecting indicators.

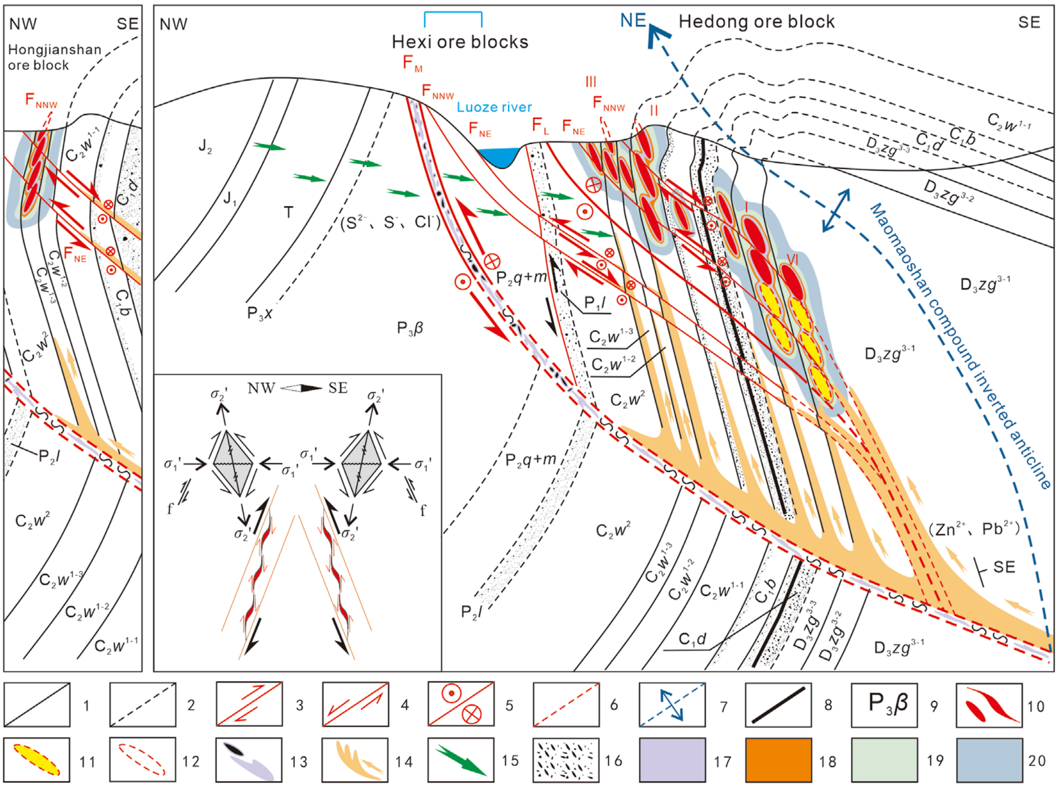

FIGURE 10
Ore-control model and mineralization–alteration zones pattern of Maoping lead–zinc deposit (According to Wu et al., 2023; Han et al. 2024). 1—Integrated contact; 2—Parallel unconformity contact; 3—Compressive fault; 4—Tensile fault; 5—Torsional fault; 6—Inferred fault; 7—Anticline; 8—Coal-bearing; 9—Formation code; 10—Known orebodies; 11—Predicting orebody; 12—Denuded orebody; 13—Dolomitization and its cemented limestone breccia; 14—Ore-forming metals fluids; 15—Reducing fluids; 16—Argillaceous and sandy clastic rock; 17—zone I; 18—zone II; 19—zone III; 20—zone IV.

6 Conclusion

From the orebodies to the wallrocks in the hanging wall, the mineralization–alteration zones of the C_2w Formation range from the massive lead–zinc ore zone (I) → lead–zinc ore veinlet + pyrite vein zone (Zone II) → spotted pyrite + striped altered dolomite zone (Zone III) → calcite veinlet + gray thick-layered dolomitic limestone zone (Zone IV). The mineralization–alteration zones of the D_3zg Formation range from the massive lead–zinc ore + massive pyrite zone (Zone I) → lead–zinc ore vein + pyrite vein zone (Zone II) → spotted pyrite + calcite stockwork/vein zone (Zone III) → calcite veinlet + masses of dolomite + gray–white cataclastic medium–coarse dolomite zone (Zone IV).

The porosity and permeability of the NW flank of the anticline are greater than those of the SE flank. On the NW flank, the greater the degree of mineralization–alteration is, the greater the porosity and permeability are, and the porosity of the orebody is lower than that during dolomitization. Tectonic activity affects the properties, migration, and precipitation of fluids, thereby controlling the alteration characteristics generated during fluid migration and changing the porosity and permeability.

During the mineralization period, the ore-forming metal fluids migrated from the deep part of the SSW region to the shallow part of the NNE region along the ore-guiding structure (Maoping Fault). Through the ore distribution structure, depressurization boiling occurred in the open space of the NE-trending interlayer sinistral compressive–torsional faults in several ore-bearing formations, resulting in fluid precipitation and the formation of different lead–zinc mineralization zones in brecciated hot-melt dolomite.

The NW flank of the Maomaoshan anticline is an important prospecting area. The pyrite + striped altered dolomite zone (Zones II–III) in the C_2w limestone and the pyrite + strong dolomite zone (Zones II–III) in the D_3zg dolomite are important prospecting indicators.

Data availability statement

The original contributions presented in the study are included in the article/Supplementary Material, further inquiries can be directed to the corresponding author.

Author contributions

JW: Conceptualization, Formal Analysis, Investigation, Methodology, Software, Validation, Visualization, Writing–original draft, Writing–review and editing. RH: Conceptualization, Data curation, Funding acquisition, Investigation, Methodology, Project administration, Resources, Supervision, Validation, Writing–review and editing. YZ: Formal Analysis, Investigation, Project administration, Resources, Writing–review and editing. PW: Formal Analysis, Investigation, Methodology, Resources, Writing–review and editing. HG: Formal Analysis, Investigation, Methodology, Writing–review and editing. LW: Formal Analysis, Investigation, Writing–review and editing. GC: Investigation, Writing–review and editing. XL: Investigation, Writing–review and editing. YY: Investigation, Writing–review and editing. YM: Investigation, Writing–review and editing.

Funding

The author(s) declare that financial support was received for the research, authorship, and/or publication of this article. This work was financed jointly by National Natural Science Foundation of China (42172086, U1133602), Yunnan Major Scientific and Technological Projects (grant no. 202202AG050014), Key Projects of School–Enterprise Cooperation (2020CHYCDZB08), Yunnan Mineral Resources Prediction and Evaluation Engineering Research Center (2011), and Yunnan Provincial Geological Process and Mineral Resources Innovation Team (2012).

Conflict of interest

The authors declare that the research was conducted in the absence of any commercial or financial relationships that could be construed as a potential conflict of interest.

Publisher's note

All claims expressed in this article are solely those of the authors and do not necessarily represent those of their affiliated organizations, or those of the publisher, the editors and the reviewers. Any product that may be evaluated in this article, or claim that may be made by its manufacturer, is not guaranteed or endorsed by the publisher.

References

Ali, S. H., Giurco, D., Arndt, N., Nickless, E., Brown, G., Demetriades, A., et al. (2017). Mineral supply for sustainable development requires resource governance. *Nature* 543 (7645), 367–372. doi:10.1038/nature21359

Bauer, T. E., Lynch, E. P., Sarlus, Z., Drejing-Carroll, D., Martinsson, O., Metzger, N., et al. (2022). Structural controls on iron oxide copper–gold mineralization and related alteration in a paleoproterozoic supracrustal belt: insights from the nautanen deformation zone and surroundings, northern Sweden. *Econ. Geol.* 117, 327–359. doi:10.5382/econgeo.4862

Chen, S. H., Han, R. S., Shentu, L. Y., Wu, P., Qiu, W. L., and Wen, D. X. (2016). Alteration zoning and geochemical element migration in alteration rock of Zhaotong lead-zinc deposit in northeastern Yunnan mineralization concentration Area. *J. Jilin Univ. (Earth Sci. Ed.)* 46 (3), 711–721. doi:10.13278/j.cnki.jjuese.201603109

Corbella, M., Ayora, C., and Cardellach, E. (2004). Hydrothermal mixing, carbonate dissolution and sulfide precipitation in Mississippi Valley-type deposits. *Miner. Deposita* 39, 344–357. doi:10.1007/s00126-004-0412-5

Cox, S. F., Knackstedt, M. A., and Braun, J. (2001). *Principles of structural control on permeability and fluid flow in hydrothermal systems*.

Han, R. S., Wu, J. B., Zhang, Y., Chen, Q., and Sun, B. T. (2024). Oblique distribution patterns and the underlying mechanical model of orebody groups controlled by structures at different scales. *Sci. Rep.* 14 (1), 4591. doi:10.1038/s41598-024-55473-z

Han, R. S., Wu, P., Wang, F., Zhou, G. M., Li, W. Y., and Qiu, W. L. (2019). Four Steps Type'ore-prospecting method for deeply concealed hydrothermal ore deposits—a case study of the Maoping Zn-Pb-(Ag-Ge) deposit in Southwestern China. *Geotecton. Metallog.* 43, 246–257. doi:10.16539/j.ddgzyckx.2019.02.005

Han, R. S., Wu, P., Zhang, Y., Huang, Z. L., Wang, F., Jin, Z. G., et al. (2022). New research progresses of metallogenic theory for rich Zn-Pb-(Ag-Ge) deposits in the Sichuang-Yunnan-Guizhou Triangle (SYGT) area, southwestern Tethys. *Acta Geol. Sin.* 96, 554–573.

Han, R. S., Zhang, Y., Ye, T. Z., Chen, Q., Ren, T., Guo, Z. L., et al. (2023). An overview of the metallogeny and geological prospecting model of Mississippi valley type (MVT) lead and zinc deposits. *Geotect. Metallogenia* 47, 915–932.

Henderson, I. H. C., and McCaig, A. M. (1996). Fluid pressure and salinity variations in shear zone–related veins, central Pyrenees, France: implications for the fault–valve model. *Tectonophysics* 262, 321–348. doi:10.1016/0040-1951(96)00018-2

Hu, R. Z., Fu, S. L., Huang, Y., Zhou, M. F., Fu, S. H., Zhao, C. H., et al. (2017). The giant South China Mesozoic low-temperature metallogenic domain: reviews and a new geodynamic model. *J. Asian Earth Sci.* 137, 9–34. doi:10.1016/j.jseaes.2016.10.016

Korges, M., Weis, P., Lüders, V., and Laurent, O. (2018). Depressurization and boiling of a single magmatic fluid as a mechanism for tin-tungsten deposit formation. *Geology* 46 (1), 75–78. doi:10.1130/g39601.1

Qiu, L., Yan, D. P., Tang, S. L., Wang, Q., Yang, W. X., Tang, X., et al. (2016). Mesozoic geology of southwestern China: indosinian foreland overthrusting and subsequent deformation. *J. Asian Earth Sci.* 122, 91–105. doi:10.1016/j.jseaes.2016.03.006

Soden, A. M., Shipton, Z. K., Lunn, R. J., Pytharouli, S. I., Kirkpatrick, J. D., Do Nascimento, A. F., et al. (2014). Brittle structures focused on subtle crustal heterogeneities: implications for flow in fractured rocks. *J. Geol. Soc.* 171, 509–524. doi:10.1144/jgs2013-051

Wang, B. L., Li, L. H., and Zeng, P. S. (2004). Basic geophysic characteristics of Sichuan-Yunnan-Guizhou rhombic block and its relationship with endo-mineralization. *J. East China Inst. Technol.* 27 (4), 301–308.

Wawrzyniec, T. F. (1999). *Dextral transcurrent deformation of the eastern margin of the Colorado Plateau (United States of America) and the mechanics of footwall uplift along the Simplon normal fault (Switzerland/Italy)*. The University of New Mexico.

Wen, D. X., Han, R. S., Wu, P., and He, J. J. (2014). Altered dolomite features and petro-geochemical prospecting indicators in the Huize lead-zinc deposit. *Geol. China* 41, 235–245.

Wibberley, C. A. J., and Shipton, Z. K. (2010). Fault zones: a complex issue. *J. Struct. Geol.* 32, 1554–1556. doi:10.1016/j.jsg.2010.10.006

Wintsch, R. P., Christoffersen, R., and Kronenberg, A. K. (1995). Fluid-rock reaction weakening of fault zones. *J. Geophys. Res. Solid Earth*, 100(B7): 13021–13032. doi:10.1029/94jb02622

Wu, H. Z., Han, R. S., Qiu, W. L., Hu, Y. Z., and Wu, P. (2015). The pore evolution of ore-bearing sandstone and its restriction to mineralization in liuju copper deposit in chuxiong basin, yunnan. *Acta Sedimentol. Sin.* 33, 512–523.

Wu, J. B., Han, R. S., Zhang, Y., Sun, B. T., Li, W. Y., Li, D. Q., et al. (2024). The fault–fold structure ore control mechanism of hydrothermal deposits——a case study of the Maoping super-large rich-Ge lead–zinc deposit in Northeastern Yunnan, China. *Ore Geol. Rev.* 168, 106039. doi:10.1016/j.oregeorev.2024.106039

Wu, J. B., Han, R. S., Zhou, G. M., Shi, Z. L., Zhang, Y., Sun, B. T., et al. (2023). Structural ore-controlling and deep prospecting direction of the Maoping Pb–Zn deposit in Northeastern Yunnan, China. *Geotect. Metallogenia* 47, 984–1001.

Wu, J. B., Pi, Q. H., Zhu, B., Hu, Y. Y., Li, G., and Wei, C. W. (2020). Late Cretaceous-Cenozoic exhumation of Northwestern Guangxi (China) and tectonic implications: evidence from apatite fission track dating. *Geochemistry* 80, 125662. doi:10.1016/j.chemer.2020.125662

Yan, D. P., Zhou, M. F., Song, H. L., Wang, X. W., and Malpas, J. (2003). Origin and tectonic significance of a mesozoic multi-layer over-thrust system within the Yangtze block (South China). *Tectonophysics* 361, 239–254. doi:10.1016/s0040-1951(02)00646-7

Zhai, Y. S. (1996). Several issues on the study of tectonic–fluid–metallogenic processes. *Earth Sci. Front.* 3, 230–236.

Zhang, R. Z. (2017). *Structural control mechanism and deep mineralization prediction of the Zhaoping gold deposit belt*. Beijing: China University of Geosciences.

Zhang, Y., Han, R. S., Ding, X., Wang, Y. R., and Wei, P. T. (2019). Experimental study on fluid migration mechanism related to Pb–Zn super-enrichment: implications for mineralisation mechanisms of the Pb–Zn deposits in the Sichuan–Yunnan–Guizhou, SW China. *Ore Geol. Rev.* 114, 103110. doi:10.1016/j.oregeorev.2019.103110

Zhang, Y., Han, R. S., and Wei, P. T. (2016). Research overview on the migration and precipitation mechanisms of lead and zinc in oreforming fluid system for carbonate-hosted lead—zinc deposits. *Geol. Rev.* 62 (1), 187–201.

Zhao, D., Han, R. S., and Ren, T. (2016). The mineralization and alteration zoning of the Le-hong lead zinc deposit, the large deposit concentration area in the Northeast of Yunnan province, China. *Bull. Mineralogy, Petrology Geochem.* 35 (6), 1258–1269.